Asociación Argentina
de Mecánica Computacional

Mecánica Computacional Vol XXXII, págs. 1825-1847 (artículo completo)
Carlos G. García Garino, Aníbal E. Mirasso, Mario A. Storti, Miguel E. Tornello (Eds.)
Mendoza, Argentina, 19-22 Noviembre 2013

# THE DETACHED INTERPHASE SIMULATION

**Santiago Márquez Damián**[a] **and Norberto M. Nigro**[a]

[a]*Centro de Investigaciones en Mecánica Computacional (CIMEC), UNL/CONICET, Colectora Ruta Nac. 168 / Paraje El Pozo, (3000) Santa Fe, Argentina, http://www.cimec.org.ar*

**Keywords:** Multiphase Flow, Algebraic Slip Mixture Model, Hyperbolic Systems

**Abstract.** This work presents a new model based on the Mixture Model and the Volume of Fluid method capable to manage flows with different scale of interphases respect to a measure of the mesh. The model relies on the concept of Detached Interphase Simulation (DIS) or the switching of the base models along the domain as an analogy of the Detached Eddy Simulation (DES) methods used for turbulence simulation. The model is implemented using the OpenFOAM® libraries and the obtained solver is then tested in several cases taken from the literature and proposed by the authors. In order to evaluate the performance of the model new quantitative measures are also proposed. The analysis of the results shows that the DIS model performs better than the base models with different levels of improvement related to the fluids density ratio.

## 1 INTRODUCTION

The multi-fluid and multi-phase systems are often present in academia and industry, setting generally a big challenge in their solution. The correct representation and solution of this kind of systems is a key knowledge in the car, atomic energy, petrochemical, naval and hydraulics, chemistry, and other industries (Brennen, 2005; Prosperetti and Tryggvason, 2007; Kolev, 2010). Throughout the years several models have been devised to simulate these phenomena, within the most often used may be: the Direct Numerical Simulation (DNS) (Scardovelli and Zaleski, 1999), the Volume of Fluid Method (VOF) (Hirt and Nichols, 1981), the Multi-fluid Method (Drew, 1983; Ishii and Hibiki, 2010) and the Mixture Model (Manninen et al., 1996). At the these days, the DNS represents the only model which is capable to afford general multi-phase/fluid problems (Scardovelli and Zaleski, 1999; Tryggvason et al., 2006); nevertheless, the present computational resources limitations turn impossible its direct application. On the other hand, due to their lack of generality, the rest of the models work only in particular cases, according to each model's hypothesis. This situation leaves an open discussion respect to the development of new models capable to manage several interface scales and/or transitions between them.

The state of the art in this topic shows that the study of the so called coupled models for the treatment of short and long scale interfaces has been in discussion in the last years. The main motivation has been the lack of precision in the solutions using the known models and the solutions given by DNS limited to low Reynolds number flows. The first work in the topic seems to be that was presented by Černe *et al.* (Černe et al., 2001), where the authors introduced a coupled method between VOF and Multi-fluid (Two-fluids) model. A model switching parameter is given by a dispersion function, $\gamma$, related to the free-surface reconstruction method, so that, there is a threshold value over which the interface is treated as having long scale and captured by VOF and the opposite case with the Two-fluids model. Since each base model is written in its original formulation there is not an unified solution framework and it is necessary to switch between models with different number of equations. This issue has particular importance in the treatment of the velocities, since the VOF model has only one velocity field meanwhile the Two-Fluids model has one velocity field per phase. The transition from two velocities to one is managed by the definition of the velocity of center-of-volume, in the opposite case the same velocity is assigned to each phase. This assumption implies some momentum equilibrium physically unrealistic and leads to lose the interface friction.

The solution of multiple scale interface problems with an unified framework was presented by Masuda and Nagaoka (Masuda and Nagaoka, 2006), who devised a coupled VOF/Multi-fluid method for the application in nozzle flows. This method recognizes four fluids, the original two fluids and two mixtures, one given by the first fluid as the dispersed phase and the other one using the second fluid as the dispersed phase. The transition between the models is governed by the dispersion function proposed by Černe *et al.*. In the same line, Štrubelj and Tiselj (Štrubelj and Tiselj, 2011), gave an unified framework for the Level-Set and the Multi-fluid method. In this approach all the scales are solved by the Multi-fluid method and an additional interface tracking term is implemented within it. The detection of the scale interfaces is achieved by the cited dispersion function.

Another example of a model based on the unified VOF/Multi-fluid approach is that was given

by Yan and Che (Yan and Che, 2010). It relies on a division of the phases by their physical state and the interface lenght scale, giving three new phases. The concept of phase division by their physical state and lenght scale was also developed by Bohorquez (Bohorquez R. de M., 2008) for the treatment of air-water-sediments in hydraulics problems. Here, there are two principal phases, the air (phase 1) and the water-sediments mixture (phase 2), the third phase are the sediments which are dispersed within the water. Thus, a VOF/ASMM model is derived in an unified framework where the large scale interphase between phase 1 and phase 2 is solved by the VOF model. The geometry of the dispersed phase (phase 3) is solved by an additional mass conservation equation without interface capturing. Since the whole model is given in the ASMM framework, only one momentum equation is solved for the air-water-sediments mixture.

From the study of the presented references is also noticeable that the field of coupled models for different interface length scales is still in development. The advances on the description of this kind of problems require the development and improvement of the models and the possibility of validation. The validation plays a crucial role, requiring more experiments and getting analytical or semi-analytical solutions. In this context the objective of this work is to present a VOF/ASMM coupled model for two phase problems and its application for academic and industrial problems. The decision respect to the use of VOF or ASMM is based on the spatial distribution of the volume fraction of fluids, as is done in the Detached Eddy Simulation (DES) (Spalart et al., 1997; Spalart, 2009) with the different eddy scales. The idea behind the model which will be presented is to treat the long scale structures of the flux purely with the VOF method. When some structures fall below the unresolved scale this zones have to be calculated using the ASMM with appropriate closure laws.

## 2 THEORETICAL FOUNDATION

### 2.1 The Algebraic Slip Mixture Model

The Algebraic Slip Mixture Model is a multi-phase model for $n$ interpenetrated phases based on the Multi-fluid model (Ishii, 1975; Ishii and Hibiki, 2010). In this model all the phases are treated as a mixture which exhibits mean properties for density and viscosity. In the Multi-fluid, model a mass and a momentum equations are solved for each phase; on the other hand, the ASMM reduces the system to a mass and a momentum equations for the whole mixture and one mass conservation equation for each of the $n-1$ phases. Since the momentum equations for these $n-1$ phases are not solved, additional *algebraic* relationships for each phase velocities with respect to the mixture velocity are given. These algebraic relationships for the slip velocities give the name to this mixture model. Finally, a closure law for all phases volume fractions is also included. Even when ASMM is physically more limited than Multi-fluid model, its results are in some particular cases comparable to that model due to the lack of closure laws available for the Multi-fluid model (Manninen et al., 1996).

The Mixture Model can be formulated using either the so called *velocity of center-of-mass*, *mixture velocity* or *mass averaged velocity*, or in terms of the *velocity of center-of-volume*. Starting from the Multi-fluid method, the velocity of center-of-mass based formulation can be

derived (Manninen et al., 1996), which is given by Eqn. (1)

$$\begin{cases} \frac{\partial}{\partial t}(\rho_m) + \vec{\nabla}\cdot(\rho_m \vec{v}_m) = 0 \\ \\ \frac{\partial}{\partial t}(\rho_m \vec{v}_m) + \vec{\nabla}\cdot(\rho_m \vec{v}_m \otimes \vec{v}_m) = -\vec{\nabla}p + \vec{\nabla}\cdot\left[\mu_m\left(\vec{\nabla}\vec{v}_m + \vec{\nabla}\vec{v}_m^{\mathrm{T}}\right)\right] + \rho_m \vec{g} \\ \\ -\vec{\nabla}\cdot\left[\rho_m c_p\left(1-c_p\right)\vec{v}_{pq}\otimes\vec{v}_{pq}\right] \\ \\ \frac{\partial}{\partial t}(\alpha_p) + \vec{\nabla}\cdot(\alpha_p \vec{v}_m) = -\vec{\nabla}\cdot\left[\alpha_p\left(1-c_p\right)\vec{v}_{pq}\right] \end{cases} \tag{1}$$

where $\rho_m = \sum_{k=1}^{n} \alpha_k \rho_k$ is the mixture density; $\vec{v}_m = \frac{\sum_{k=1}^{n} \alpha_k \rho_k \vec{v}_k}{\rho_m}$ is the velocity of center-of-mass, which is calculated from the phase velocities $\vec{v}_k$, the fractions $\alpha_k$ (which obey the closure law $\sum_{k=1}^{n} \alpha_k = 1$) and the densities $\rho_k$; $p$ is the pressure, which is common for all the phases; $\mu_m = \sum_{k=1}^{n} \alpha_k \mu_k$ is the dynamic viscosity of the mixture; $\vec{g}$ is the gravitational acceleration; $c_k = \frac{\alpha_k \rho_k}{\rho_m}$ is the mass fraction for the phase $k$ and $\vec{v}_{pq} = \vec{v}_p - \vec{v}_q$ is the relative velocity for a given phase, $p$, with respect to another phase, $q$. This relative velocity can be calculated by algebraic expressions related to the physics of the dispersed phase. For the sake of simplicity, it is convenient to set a general constitutive law for the relative velocity, $\vec{v}_{pq}$, as it is shown in Eqn. (2)

$$\vec{v}_{pq} = \vec{v}_{rc}\ (1-\alpha_p)^a \tag{2}$$

where $\vec{v}_{rc}$ and $a$ are constants for the model. The $\vec{v}_{rc}$ constant can be interpreted as the velocity of a single bubble or droplet moving in the continuum phase. This expression is flexible and allows to match several other models, for example the Schiller & Naumann drag law (Schiller and Naumann, 1935) can be fitted by selecting an appropriate value for $v_{rc}$ and with $0 \leqslant a \leqslant 1$. In addition, Ishii & Hibiki (Ishii and Hibiki, 2010) provide a complete reference for drag laws in several industrial cases. Finally, the momentum equation has an extra term accounting for the momentum exchanging between the phases, which is calculated by the drift tensor, $\overline{\overline{\tau_D}}$ in Eqn. (3)

$$\overline{\overline{\tau_D}} = \rho_m c_p\left(1-c_p\right)\vec{v}_{pq}\otimes\vec{v}_{pq} \tag{3}$$

The resulting system is composed by the mass conservation equation for the mixture, the momentum equation for the mixture velocity and the mass conservation equation for the secondary phase $p$ in a two-components mixture ($p$ and $q$), where the $p$ phase is the dispersed one. This system of three equations has three unknowns, which are: $\vec{v}_m$, $p$ and $\alpha_p$. Respect to $\rho_m$ it is linked to $\alpha_p$ via its constitutive equation. As it is usual in incompressible problems the pressure has no evolution equation, so that it becomes a Lagrange multiplier for the restriction given by the mixture density transport equation. This characteristic leads to a pressure-velocity coupling that can be treated in several ways, as the Fractional-Step or PISO/SIMPLE like methods (Gastaldo et al., 2008) among others. This issue appears also in reacting flows (Babik et al., 2005; Najm et al., 1998; Knio et al., 1999), the Low-Mach solvers applied in that problems are also an inspiration for the solution of ASMM problems. In addition $\alpha_p$ has to be bounded in the [0, 1] interval to have physical meaning. Since $v_m$ is not divergence free and that the momentum and mixture conservation equations depend on $\alpha_p$ the boundedness is not a direct consequence of the correct discretization of the third equation in Eqn. (1), but of the whole system (Gastaldo

et al., 2011).

As was stated previously, another formulation can be devised for ASMM in terms of the velocity of the center-of-volume or the *volumetric flux*. To do so it is necessary to find a relationship between the velocity of center-of-mass and this new velocity (Bohorquez, 2012; Márquez Damián, 2013). The desired relationship is shown in Eqn. (4)

$$\vec{v}_m = \vec{u} + \alpha_q \, (1 - \alpha_q) \, \frac{\rho_q - \rho_p}{\rho_m} \, \vec{v}_{qp} \tag{4}$$

Now, starting from the Multi-fluid method it is possible to find a new mass conservation equation for the mixture written in terms of the velocity of center-of-volume. Then, for a given phase $k$ of the system the mass conservation equation (without sources) reads as in Eqn. (5)

$$\frac{\partial \alpha_k \rho_k}{\partial t} + \vec{\nabla} \cdot (\alpha_k \rho_k \vec{v}_k) = 0 \tag{5}$$

assuming constant densities for all phases, dividing each mass conservation by its corresponding density and then summing over all phases and recalling that $\sum_{k=1}^{n} \alpha_k = 1$, the final expression is given by Eqn. (6)

$$\vec{\nabla} \cdot \vec{u} = 0 \tag{6}$$

where $\vec{u} = \sum_{k=1}^{n} \alpha_k \vec{v}_k$ is the velocity of center-of-volume. Now, taking a bi-phasic system, the mass conservation equation for the primary (continuum) phase can be obtained and the relationship given in Eqn. (7) can be derived,

$$\vec{v}_q = \vec{u} + (1 - \alpha_q) \, \vec{v}_{qp} \tag{7}$$

Replacing this expression in Eqn. (5) for the $q$ phase allows to write the final expression for the mass conservation equation for the $q$ phase, Eqn. (8),

$$\frac{\partial \alpha_q}{\partial t} + \vec{\nabla} \cdot (\alpha_q \vec{u}) + \vec{\nabla} \cdot [\alpha_q \, (1 - \alpha_q) \, \vec{v}_{qp}] = 0 \tag{8}$$

Finally, the mixture momentum equation can be rewritten in terms of the primary phase void fraction $\alpha_q$ and the relative velocity of the primary phase with respect to the secondary one $\vec{v}_{qp}$. Starting from the expression of the drift tensor in Eqn. (3), taking into account that $\vec{v}_{qp} = -\vec{v}_{pq}$ and $\alpha_q = 1 - \alpha_p$ and doing some algebraic simplifications, it becomes which is shown in Eqn. (9)

$$\overline{\overline{\tau_{\mathrm{D}}}} = \rho_m c_p \, (1 - c_p) \, \vec{v}_{pq} \otimes \vec{v}_{pq} = \alpha_q \, (1 - \alpha_q) \, \frac{\rho_q \, \rho_p}{\rho_m} \vec{v}_{qp} \otimes \vec{v}_{qp} \tag{9}$$

In order to give stability to the solution and to simplify the definition of the boundary conditions (Berberovic et al., 2009) the treatment of the pressure terms is performed using the modified pressure $p_{rgh}$ defined in Eqn. (10)

$$p_{rgh} = p - \rho_m \vec{g} \cdot \vec{x} \tag{10}$$

where $\vec{x}$ is the position vector. Thus, the pressure gradient is then expressed as in Eqn. (11)

$$-\vec{\nabla} p = -\vec{\nabla} p_{rgh} - \vec{g} \cdot \vec{x} \vec{\nabla} \rho_m - \rho_m \, \vec{g} \tag{11}$$

regrouping terms the Eqn. (12) is obtained

$$-\vec{\nabla}p + \rho_m\,\vec{g} = -\vec{\nabla}p_{rgh} - \vec{g}\cdot\vec{x}\vec{\nabla}\rho_m \tag{12}$$

which allows to replace the pressure gradient and gravity terms in the second equation of Eqn. (13) by a function of the modified pressure.

In summary, the continuity equation and the momentum balance for the mixture and the mass conservation equation for the primary phase in center-of-volume based formulation may be written as in Eqn. (13)

$$\begin{cases} \vec{\nabla}\cdot\vec{u} = 0 \\ \\ \frac{\partial}{\partial t}(\rho_m\vec{v}_m) + \vec{\nabla}\cdot(\rho_m\vec{v}_m\otimes\vec{v}_m) = -\vec{\nabla}p_{rgh} + \vec{\nabla}\cdot\left[\mu_m\left(\vec{\nabla}\vec{v}_m + \vec{\nabla}\vec{v}_m^{\mathrm{T}}\right)\right] - \vec{g}\cdot\vec{x}\vec{\nabla}\rho_m - \\ \qquad\qquad \vec{\nabla}\cdot\left[\alpha_q\,(1-\alpha_q)\,\frac{\rho_q\,\rho_p}{\rho_m}\vec{v}_{qp}\otimes\vec{v}_{qp}\right] \\ \\ \frac{\partial\alpha_q}{\partial t} + \vec{\nabla}\cdot(\alpha_q\vec{u}) + \vec{\nabla}\cdot\left[\alpha_q\,(1-\alpha_q)\,\vec{v}_{qp}\right] = 0 \end{cases} \tag{13}$$

The principal advantage of this method is the possibility to use a divergence free velocity in the mass conservation equation for the primary phase. In addition, it is then possible to avoid solving a mass conservation equation for $\rho_m$ which is no more an unknown but a derived quantity from $\rho_q$, $\rho_p$ and $\alpha_q$. On the other hand, this system has a mixed formulation between center-of-volume and center-of-mass velocities which requires transformation formulas in order to solve the momentum equation and perform the pressure-velocity coupling loop, these formulas are based in Eqn. (4).

## 2.2 The Volume of Fluid method as a Mixture Model

The VOF method can be classified as a interface capturing technique which implies that the free-surface is not exactly tracked by the mesh like in interface tracking methods, but its position is approximated by a phase fraction function (Carrica et al., 2006). In this sense, the phase fraction function plays the same role as in ASMM. This similarity can be exploited in view of the unified framework needed for an extended mixture model.

So that, it would be valuable to find a derivation of the VOF method from the ASMM. This sets a difference with respect to the original approach given by Hirt & Nichols (Hirt and Nichols, 1981) in the presentation of the method. This derivation allows to understand the similarities between both methods and the potential for an unified framework and solver. The derivation of the VOF method starts recalling the center-of-volume formulation of the ASMM, as is presented in Eqn. (13). A principal difference between ASMM and the VOF method is that the VOF method considers a continuous velocity field along all the interfaces, which is consistent with the interface boundary conditions given by the physics of fluids. This is possible since all the interfaces are supposed to be resolved at DNS scale. This hypothesis implies that the relative velocity between phases is null, $\vec{v}_{qp} = 0$. By inspection of the momentum equation given in the system of Eqn. (13) it is clear that the drift tensor $\overline{\overline{\tau_{\mathrm{D}}}} = \alpha_q\,(1-\alpha_q)\,\frac{\rho_q\,\rho_p}{\rho_m}\vec{v}_{qp}\otimes\vec{v}_{qp}$ is also null. In addition, the possibility of capturing long-scale interfaces allows to model the

effects of the surface tension. This effect is modeled by the Continuum Surface Model (CSF) (Brackbill et al., 1992) which adds to the momentum equation the term given in Eqn. (14)

$$\vec{F}_\sigma = \sigma\kappa\vec{\nabla}\alpha_q \tag{14}$$

where $\kappa$ is the mean curvature of the free surface which is given by Eqn. (15)

$$\kappa = \vec{\nabla}\cdot\left(\frac{\vec{\nabla}\alpha_q}{\left|\vec{\nabla}\alpha_q\right|}\right) \tag{15}$$

Finally, it is important to note that the third equation of Eqn. (13) can be also simplified since the nonlinear term is zero due to the null relative velocity $\vec{v}_{qp}$. This term is deliberately included in the formulation with the aim to compress the interface. It is worthy to note that since in VOF method $\alpha_q$ is expected to be ever valued 0 or 1, except for the interfaces, this term acts only on this place (Berberovic et al., 2009; Rusche, 2002; OpenCFD, 2005; Weller, 2008) and vanishes otherwise, so the original formulation for VOF is recalled in general and the non-linear term is used only at interface zones. Thus, the solved system reads as in Eqn. (16)

$$\begin{cases} \vec{\nabla}\cdot\vec{u} = 0 \\ \\ \frac{\partial}{\partial t}(\rho_m\vec{u}) + \vec{\nabla}\cdot(\rho_m\vec{u}\otimes\vec{u}) = -\vec{\nabla}p_{rgh} + \vec{\nabla}\cdot\left[\mu_m\left(\vec{\nabla}\vec{u} + \vec{\nabla}\vec{u}^{\mathrm{T}}\right)\right] - \vec{g}\cdot\vec{x}\vec{\nabla}\rho_m + \sigma\kappa\vec{\nabla}\alpha_q \\ \\ \frac{\partial\alpha_q}{\partial t} + \vec{\nabla}\cdot(\alpha_q\vec{u}) + \vec{\nabla}\cdot\left[\alpha_q\left(1-\alpha_q\right)\vec{v}_{qp}\right] = 0 \end{cases} \tag{16}$$

This formulation will hereinafter referred as the Weller-VOF method.

### 2.3 A coupled model

From the comparison of the systems given in Eqn. (13) and Eqn. (16), it becomes clear that both VOF and ASMM models can be written in a very close formulation, and even more, the VOF model can be directly derived from the ASMM. The basic differences between these approaches in the context of the mixture models are the terms related to the different scales. So that, since the interfaces are supposed to be completely captured, the VOF model has a term in the momentum equation including the effects of the surface tension. On the other hand, the ASMM does not include this term; however, it takes into account the effect of the drift stresses, or the effect of the small scale interfaces. In addition, the relative velocity between phases has physical meaning in ASMM while in VOF it is only a numerical tool in order to compress the interface. So that, using $\theta$ as a flag to activate or deactivate certain terms according to the interface scale which is being resolved, VOF (Weller-VOF) and ASMM can be coupled as in

Eqn. (17)

$$\begin{cases} \vec{\nabla}\cdot\vec{u}=0 \\ \\ \frac{\partial}{\partial t}(\rho_m\vec{v}_m)+\vec{\nabla}\cdot(\rho_m\vec{v}_m\otimes\vec{v}_m)=-\vec{\nabla}p_{rgh}+\vec{\nabla}\cdot\left[\mu_m\left(\vec{\nabla}\vec{v}_m+\vec{\nabla}\vec{v}_m^{\mathrm{T}}\right)\right]-\vec{g}\cdot\vec{x}\vec{\nabla}\rho_m \\ +\theta\,\sigma\kappa\vec{\nabla}\alpha_q-(1-\theta)\,\vec{\nabla}\cdot\left[\alpha_q\,(1-\alpha_q)\,\frac{\rho_q\,\rho_p}{\rho_m}\vec{v}_{qp}\otimes\vec{v}_{qp}\right] \\ \\ \frac{\partial\alpha_q}{\partial t}+\vec{\nabla}\cdot(\alpha_q\vec{u})+\vec{\nabla}\cdot\{\alpha_q\,(1-\alpha_q)\,[\theta\,\vec{v}_{qp,\mathrm{VOF}}+(1-\theta)\,\vec{v}_{qp,\mathrm{ASMM}}]\}=0 \end{cases} \tag{17}$$

where $\vec{v}_{qp,\mathrm{VOF}}$ and $\vec{v}_{qp,\mathrm{ASMM}}$ are the relative velocities calculated either numerically or physically. The value of $\theta$ coefficient is $\theta=1$ for VOF and $\theta=0$ for ASMM. Two methodologies to calculate $\theta$ are studied, in order to select the most convenient for the proposed algorithm.

One of the available criteria for long and short scale models coupling, used by several authors, was given by Cerne (Černe et al., 2001). It is based on the analysis of the frame obtained taking into account a given cell and all it neighbors by faces and edges. The switching function $\gamma$ is obtained finding the minimum of the function $G$ as is shown in Eqns. (18-19)

$$G_{i,j}\left(\vec{n}\right)=\sum_{l=-1}^{1}\sum_{k=-1}^{1}\left(\alpha_{q,i+k,j+l}-\alpha'_{q,i+k,j+l}\left(\vec{n}\right)\right)^2 \tag{18}$$

$$\gamma_{i,j}=\min\left(G_{i,j}\left(\vec{n}\right)\right) \tag{19}$$

Finally, it is necessary to set a threshold value for $\gamma=\gamma_0$ such that the $\theta$ criterion could be calculated as in Eqn. (20)

$$\theta=\begin{cases} 1,\ \text{if}\ \gamma_{\mathrm{i,j}}<\gamma_0 \quad [\text{VOF in cell (i, j)}] \\ \\ 0,\ \text{if}\ \gamma_{\mathrm{i,j}}>\gamma_0 \quad [\text{Multi}-\text{fluid in cell (i, j)}] \end{cases} \tag{20}$$

The threshold value is obtained by several cases study, such that the recommended value is $\gamma_0\cong 0.6$ (Černe et al., 2001). This methodology is attractive since it is based in the reconstruction of the interface (Puckett et al., 1997), but requires the time consuming solution of a minimization problem at each cell and time-step.

Another criterion can be devised based on the gradient of the phase fraction function $\alpha_q$ calculated by the cell-centered Finite Volume Method (FVM) (Jasak, 1996; Márquez Damián, 2013), which is shown in Eqn. (21)

$$\vec{\nabla}\alpha=\frac{1}{V}\sum_f\left(\alpha_q\right)_f\cdot\vec{S}_f \tag{21}$$

where $V$ is the volume of a given cell, $f$ is an index along all the faces of the cell and $\vec{S}_f$ is the face area vector. As a next step, this gradient is interpolated at faces obtaining $\vec{\nabla}\alpha_f$. The gradient at the faces gives a general idea of the variation of the phase fraction along the domain. Large gradients are associated to big changes in $\alpha$, and then a large scale interface is inferred.

This value is weighted with a measure of the mesh in order to normalize the switching function. A clear local jump between two phases requires not only a big gradient but also to be extended in few cells. So that, the gradient is multiplied by the face's neighboring cells center-to-center vector, $\vec{d}_{PN}$ as is shown in Eqns. (22)-(23) (See Figure 1)

$$\vec{d}_{PN} = \vec{x}_P - \vec{x}_N; \tag{22}$$

$$\gamma_f = |\vec{\nabla}\alpha_f \cdot \vec{d}_{PN}| \tag{23}$$

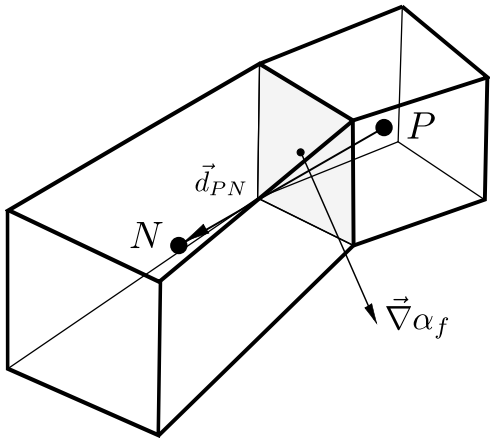


Figure 1: Face gradient criterion

Finally, the criterion to switch between VOF and ASMM is given by the rules expressed in Eqn. (24). It states that VOF will be used in high relative gradient zones (large scale interfaces) and in regions with $\alpha \cong 1$ or $\alpha \cong 1$, indicating pure phases; in all other cases, ASMM will be used. This criterion requires the selection of $\gamma_0$, the threshold for small gradients and $\epsilon$, which is a magnitude that controls the maximum deviation from $\alpha = 1$ or $\alpha = 0$ to be considered as a pure phase.

$$\theta_f = \begin{cases} 1, \text{ if } \alpha_f < 0 + \epsilon \text{ o } \alpha_\text{f} > 1 - \epsilon & [\text{VOF in face } f] \\ 1, \text{ if } \gamma_f > \gamma_0 & [\text{VOF in face } f] \\ 0, \text{ if } \gamma_f < \gamma_0 & [\text{ASMM in face } f] \end{cases} \tag{24}$$

The values for $\gamma_0$ and $\epsilon$ have to be adjusted according to the problem. Since in VOF the interface is resolved in about three cells a reference value is $\gamma_0 = 0.33$. Respect to $\epsilon$, a typical value is $\epsilon = 5 \times 10^{-3}$. The principal advantages of this indicator function are its intrinsic 3D formulation and its simplicity and low demanding calculation. This method will be then used for model switching.

## 3 A PISO SOLVER FOR THE EXTENDED MODEL

The derivation of a solver for the Extended Model is based on the solver for the Weller-VOF method given in the OpenFOAM® suite, which is called `interFoam`. It relies on a pressure-velocity coupling based on a PISO (Pressure Implicit Split of Operators) loop (Issa,

1986; Jasak, 1996; Peng Karrholm, 2008). In addition it is necessary to solve the $\alpha_q$ equation which is achieved by means of the Multidimensional Universal Limiter for Explicit Solution (MULES) an explicit solver based on the Flux Corrected Transport (FCT) technique (Zalesak, 1979; Rudman, 1997; Márquez Damián, 2013). The use of the MULES integrator gives a bounded value for $\alpha_q^{n+1}$ and returns a limited version of the flux used in the integration, $\mathrm{F}_{\alpha_q}$, which is needed to assemble the momentum equation. In addition, the solution method of the system given in Eqn. (16) includes an adaptive time-step control and the sub-cycling in the solution of $\alpha_q$ equation (Berberovic et al., 2009). This sub-cycling is performed in order to give stability to the solution of the $\alpha_q$ equation, so that choosing a number of sub-cycles $n_{sc}$ the sub-step is defined as $\Delta t_{sc} = \frac{\Delta t}{n_{sc}}$.

Since the flux used in the integration of the $\alpha_q$ equation is based on a center-of-volume velocity, it is necessary to give a center-of-mass velocity flux of mass flux in order to be able to assemble the momentum equation. This mass flux has to be calculated carefully within each sub-cycle. The basic assembling of this flux is given by the relationship between the center-of-mass velocity and the center-of-volume velocity and is necessary since the $\alpha_q$ equation modifies the mass distribution, so that recalling Eqn. (4) and assembling a mass face flux, it becomes as is shown in Eqn. (25)

$$F_{\rho m,sc,i} = \mathrm{F}_{\alpha_q} \left(\rho_q - \rho_p\right) + F\, \rho_p \tag{25}$$

where $F^n = \vec{u}_f \cdot \vec{S}_f$ is the flux of the center-of-volume velocity. So that, in each sub-cycle a partial mass flux is assembled as $F_{\rho m,sc,i}$. The mass flux for the complete time-step is obtained by the discrete integral form of the mean value theorem as in Eqn. (26)

$$F_{\rho m} = \sum_{i=1}^{n_{sc}} \frac{\Delta t_{sc}}{\Delta t} F_{\rho m,sc,i} \tag{26}$$

Once the $\alpha_q$ is solved it is necessary to assemble and solve the discretized version of the momentum equation in order to obtain a prediction of the center-of-mass velocity; this step is called the momentum predictor (`momentumPredictor`). This equation is shown in Eqn. (27)

$$\begin{aligned} &\tfrac{\rho_m^{n+1}\tilde{\vec{v}}_m - \rho_m^n \vec{v}_m^n}{\Delta t} V + \textstyle\sum_f F_{\rho_m}^{n+1} \vec{v}_m \cdot \vec{S}_f = \textstyle\sum_f \left(\mu_m^{n+1}\right)_f \left(\vec{\nabla}\vec{v}_m\right)_f \cdot \vec{S}_f + \left(\vec{\nabla}\vec{v}_m^n \cdot \vec{\nabla}\mu_m^{n+1}\right) V \\ &- \textstyle\sum_f \left(1-\theta_f\right) \left[\alpha_q^{n+1} \left(1-\alpha_q^{n+1}\right) \frac{\rho_q \rho_p}{\rho_m^{n+1}} \vec{v}_{qp}^n \otimes \vec{v}_{qp}^n\right]_f \cdot \vec{S}_f + \mathcal{R}\left\{\theta_f \left(\sigma\kappa\right)_f \left(\vec{\nabla}\alpha_q^{n+1}\right)_f \right. \\ &\left. - \left[\left(\vec{g}\cdot\vec{x}\right)_f \left(\vec{\nabla}\rho_m^{n+1}\right)_f - \left(\vec{\nabla}p_{rgh}^n\right)_f\right] \left|\vec{S}_f\right|\right\} \end{aligned} \tag{27}$$

where $F_{\rho_m}$ is the mass face flux given by $F_{\rho_m} = \left(\rho_m \vec{v}_m\right)_f \cdot \vec{S}_f$ and $\vec{a} = \mathcal{R}\left(\vec{a}\cdot\vec{S}_f\right)$ is an operator to reconstruct cell-centered fields from fields given as fluxes at faces.

In order to be able to obtain a PISO loop for the correction of the predicted center-of-mass velocity and the calculation of the modified pressure $p_{rgh}$ it is necessary to have a flux relationship between the velocity of center-of-mass and the velocity of center-of-volume and to define

a pressure equation. So that, starting from Eqn. (4), isolating $\vec{u}$ and multiplying by the face area vector the desired flux relationship is obtained in Eqn. (28)

$$F = \vec{u}_f \cdot \vec{S}_f = (\vec{v}_m)_f \cdot \vec{S}_f - \left[\alpha_q \left(1 - \alpha_q\right) \frac{\rho_q - \rho_p}{\rho_m}\right]_f (\vec{v}_{qp})_f \cdot \vec{S}_f \tag{28}$$

Following the derivation of the pressure equation in standard PISO method, a pressure equation is obtained for the extended model (Márquez Damián, 2013), as is shown in Eqn. (29). This expression includes the effect of the gravitational acceleration and the surface tension.

$$\sum_f \left[\left(\frac{1}{a_P}\right)_f \left(\vec{\nabla} p_{rgh}^{\nu+1}\right)_f\right] \cdot \vec{S}_f = \sum_f \left[\left(\frac{\vec{H}(\vec{v_m})}{a_P}\right)_f + \theta_f \left(\sigma\kappa\right)_f \left(\vec{\nabla}\alpha_q^{n+1}\right)_f - \left(\vec{g}\cdot\vec{x}\right)_f \left(\vec{\nabla}\rho_m^{n+1}\right)_f\right] \cdot \vec{S}_f - \sum_f \left[\alpha_q \left(1-\alpha_q\right) \frac{\rho_q - \rho_p}{\rho_m}\right]_f (\vec{v}_{qp})_f \cdot \vec{S}_f \tag{29}$$

In addition, the relationship given by Eqn. (28) allows to solve the phase fraction transport equation, the third equation in Eqn. (17), using a conservative flux for $\vec{u}$ assembled from the flux of $\vec{v}_m$ given by the last PISO loop.

Given the formulation of the coupled model and the auxiliary equations needed for the pressure-velocity coupling is now possible to describe the solver algorithm for the extended model, which is as follows:

1. Solve the mass conservation equation for the primary phase for ${\alpha_q}^{n+1}$ [discretized version of the third equation in Eqn. (17)], assemble the mass face flux ${F_{\rho m}}^{n+1}$ [Eqn. (26)] and get the new mixture density ${\rho_m}^{n+1}$
2. Solve the momentum predictor [Eqn. (27)] for $\tilde{\vec{v}}_m$
3. Do the PISO loop to find the modified pressure by means of Eqn. (29), the mass flux and the velocity of center of mass
4. The face flux for the velocity of center-of-volume is recovered from the flux using Eqn. (28)
5. Return to step 1 until finish.

## 4 EXAMPLES

### 4.1 Interaction of a bubble plume with the water surface

The first example gives a semi-quantitative validation from the phenomenon of interaction of a bubble plume and the water surface. This phenomenon appears in blowouts in offshore drilling, broken gas pipelines and natural undersea gas releases forming big bubble plumes. In addition, bubble plumes of small extension are used for mixing process in reservoirs or waste water treatment, chemical reactors and metallurgical processes (Friedl and Fanneløp, 2000; Zanotti, 2007).

The example is taken from the work of Friedl and Fanneløp (Friedl and Fanneløp, 2000) and consists of the generation of a bubble plume in laboratory conditions released from the bottom

of a water pool, as is shown in Figure 2. The pool has a square cross-section of 1[1] of side and 0.95 in height. The free surface is set at $H_v = 0.66$. The air is released from the bottom of the tank through a square duct of area $A_i = 0.0005067$ and lenght of $h_i = 0.04502$ with a release velocity of $v_i = 2.6$ which corresponds to the case a4 of the reference. The physical properties of the fluids are as follows: the density of the water, $\rho_q = 1000$, the kinematic viscosity of the water $\nu_q = 1 \times 10^{-6}$, the density of the air $\rho_p = 1$, the kinematic viscosity of the air $\nu_q = 1.48 \times 10^{-5}$ and the surface tension $\sigma = 0.07$. The gravitational acceleration is $\vec{g} = (0, 0, -9.81)$.

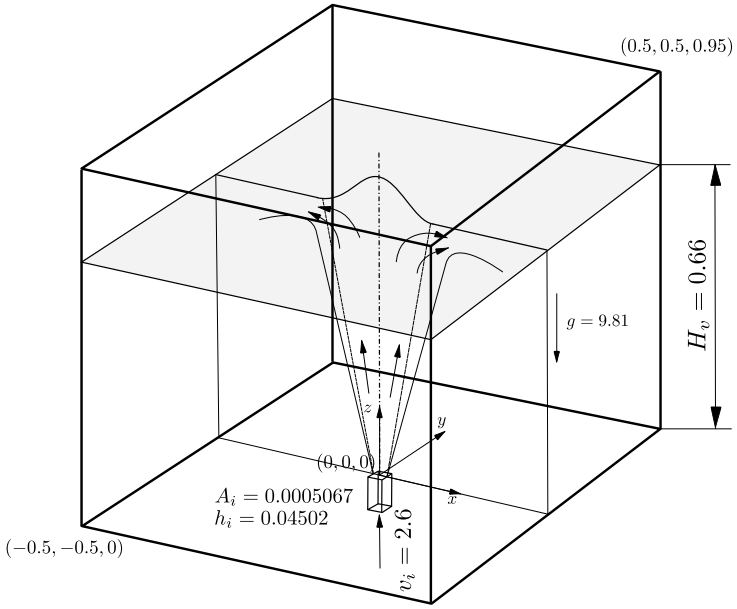


Figure 2: Geometry for the a4 case of bubble plume in (Friedl and Fanneløp, 2000). $A_i$ and $h_i$ are the cross section and height of the inlet duct. The shaded zone indicates the original free surface position and the bell-shaped curve of the mean free surface for the $x - z$ plane

As is expected, when the bubble plume reaches the free surface it is disturbed forming a fountain with different shapes but having in common a greater disturbance near the center of the fountain, and then decaying to the sides of the pool, as is shown in Figure 2.

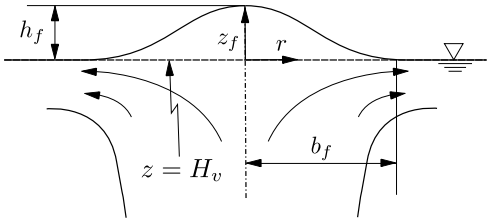


Figure 3: Mean shape of the fountain presented in Figure 2 [adapted from (Friedl and Fanneløp, 2000)]

[1] All the magnitudes are expressed in the International System of Units

The results reported in the reference are an average of the experimental results which can be fitted by a bell-shaped function as in Figure 3. The expression of the mean free surface shape on a given vertical plane ($x - z$ in the figure) is presented in Eqn. (30)

$$h(r) = h_f \, \mathrm{e}^{-r^2/b_f^2} \tag{30}$$

where $h$ is the height of the mean free surface for a given radius $r$ (the fountain is considered to be circular), $h_f$ is the maximum height of the fountain and $b_f$ is the semi-diameter of the fountain.

So that, two series of simulations were performed, the first one with the standard VOF solver (`interFoam`[2]) and the second one with the extended model. Each series had three cases with similar settings but with different size hexahedral meshes: a) meshed with `blockMesh` with 364,000 elements; b) meshed in Gambit® with 574,975 elements, with local mesh refinement for a better capturing of the plume and the free surface; c) a mesh resulting of the subdivision by two in the three directions of the previous mesh using the tool `refineMesh`, giving a mesh with 4,599,800 elements and the same refinement properties of the original mesh.

With respect to the boundary conditions for $\alpha_q$, a zero gradient was set at all walls except for the top and the inlet. On the top, a mixed boundary condition was set using a fixed value of zero if the flux is ingoing, and zero gradient for $\alpha_q$ if the flux is outgoing. At the inlet, the value of $\alpha_q$ was fixed as $\alpha_q = 0$ to ensure a pure air inlet. The boundary conditions for the modified pressure they were set as $\vec{\nabla} p_{rgh} \cdot \vec{S}_f = -\vec{\nabla} \rho \, |\vec{g}| \cdot \vec{S}_f$ for all the walls and the inlet. At the top the boundary condition was set with a total pressure of zero. Finally, for the center-of-volume velocity the non-slip boundary condition was set for all walls except for the top and the inlet. At the top the velocity gradient was set as zero for outgoing flows and the value of the velocity as zero for ingoing flows. The inlet was set with a fixed velocity $\vec{u} = (0, 0, 2.6)$. The relative velocity law needed by the zones solved with ASMM in the coupled model was set with $a = 0$, see Eqn. (2), giving a constant velocity. The value for this constant velocity was reported in the reference as $v_{qp} = 0.35$. The parameters for model coupling were set as $\gamma_0 = 0.025$ and $\epsilon = 5 \times 10^{-3}$ after a brief optimization of the results.

The first case (VOF with coarse mesh) was run until $t = 10$ in order to reach the full development of the bubble plume; then, it was run to $t = 20$. The left runnings were done mapping the coarse mesh solution for $t = 10$ into the finer meshes and then running until $t = 20$. For all the calculation of the mean values reported for the experiments the interval $t = 10{-}20$ was used.

The general results are reported in Figure 4 for VOF, and in Figure 5 for the extended model. From the first figure, it is clear that the coarse mesh captures few details of the surface mesh; in addition, the pool has non-physical chunks spread at the sides of the plume (the grayscale has been saturated to white at $\alpha_q = 0.8$ in order to easily see the gas zones). The refinement of the mesh in b) and c) improves the surface capturing but at the same time the VOF method increases its ability to capture the break-up of the big bubbles. The break-up gives small chunks and bubbles which are not correctly removed by buoyancy and then stay in the pool advected by the lateral flow from the plume to the sides. It is expected that successive mesh refinements allow capturing the fine bubbles dynamics, as will be presented for the Dam Break case. The

[2]The words in courier font corresponds to OpenFOAM®'s utilities or commands

observation of the pictures from the experimental work confirms that the bubbles concentrate around the plume and there is no recirculation [see Figure 3.3 in (Friedl, 1998)]. On the other hand, Figure 5 represents the solution for the three meshes with the extended model, where the effect of the mesh refinement is clear again. At the same time, the fragmented chunks are properly removed by the activation of the ASMM giving a clear plume and keeping the pool free of zones without physical meaning.

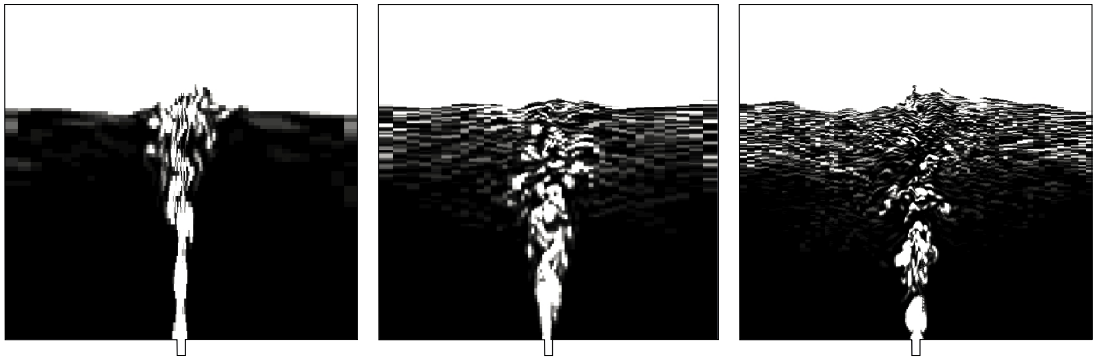


Figure 4: Solution for the bubble plume with VOF for three different meshes, a) coarse, b) fine, c) finest. The grayscale is saturated to white at $\alpha_q = 0.8$

In addition to this qualitative analysis the mean shape of the free surface can be compared with the expression given in Eqn. (30). The results are presented in Figure 6, where it is possible to appreciate the effect of the refinement. The reconstruction of the free surface is similar in both of the models showing that the extended method retains the surface capturing capabilities of the VOF model. In addition, comparing the numerical solutions to the experimental fitted curve it is clear that the fountain width is underestimated in both of the models. This effect is attributable to the lack of turbulent dispersion modeling. Here is important to note that the VOF model includes the effects of the turbulence only in the momentum equation in order to model the non-resolved scales of eddies. The scales of the interface are supposed to be captured by the mesh, so no diffusion term is added in the conservation equation of the void fraction.

### 4.2 Dam Break with degassing

The second example is the Dam Break problem, which is widely used as test problem for multi-phase solvers (Martin and Moyce, 1952; Cruchaga et al., 2007). In this case, a cavity is filled by the less dense fluid and a column of the more dense fluid is formed in a corner. This column suddenly collapses evolving within the cavity with waves and splashing which causes mixing between the fluids. In this case an obstacle has been added in order to assure stronger agitation and mixing. The final state is logically a quiescent pool with the more dense fluid at the bottom and the less dense fluid at the top.

The Dam Break is solved first by the VOF method in the domain $[0, 0] \times [0.584, 0.584]$ with an hexahedral mesh of approximately $720 \times 688$ (495360) elements, see Figure 7). The physical parameters for the fluids are $\rho_q = 1000$, $\nu_q = 1 \times 10^{-6}$ and $\rho_p = 1$, $\nu_p = 1.48 \times 10^{-5}$ with

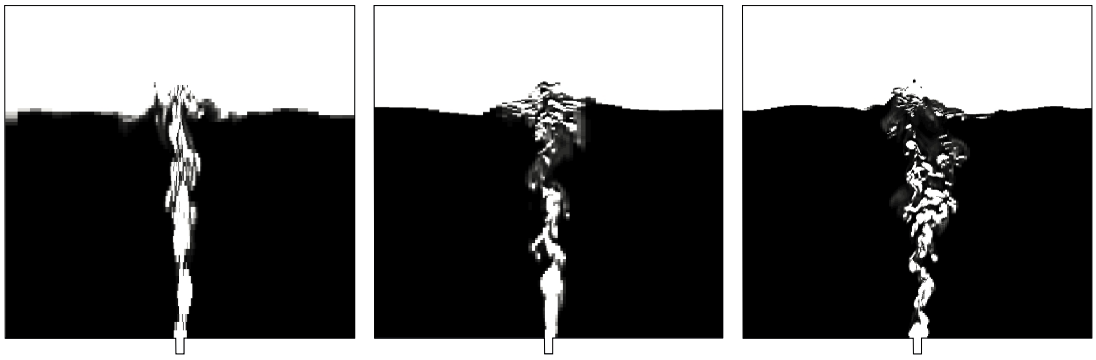


Figure 5: Solution for the bubble plume with the extended model for three different meshes, a) coarse, b) fine, c) finest. The grayscale is saturated to white at $\alpha_q = 0.8$

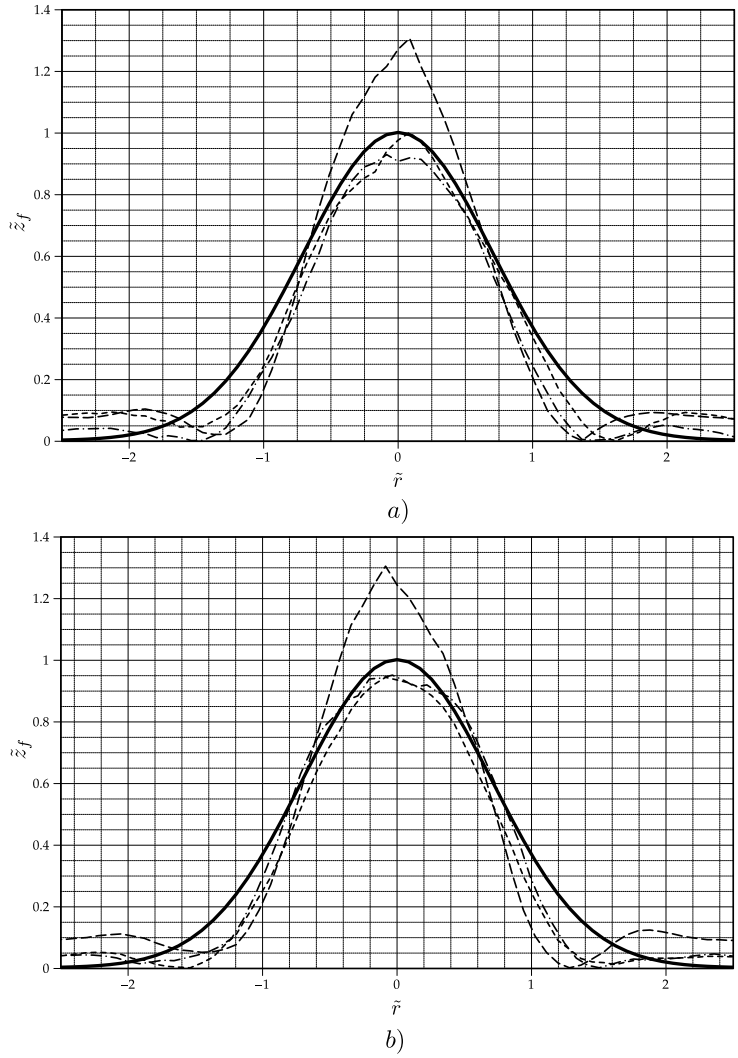


Figure 6: Mean surfaces for the bubble plume with a) VOF, b) Extended Model. ——— free surface theoretical model; — — — coarse mesh; — — — — fine mesh; ——— · ——— finest mesh

a surface tension $\sigma = 0.07$. The gravity is set as $\vec{g} = (0, -9.81, 0)$. The solution domain is filled with the less dense fluid except for the area given by $[0, 0] \times [0.1461, 0.438]$ where the more dense fluid is located. This rectangle gives the initial condition of the water column that collapses at the beginning of the simulation.

With respect to the boundary conditions, these are similar to which were used in the last example, in the case of the walls and top side. As the mesh has a dummy third dimension, $z$, front and back boundaries were set such that all the corresponding terms and the derivatives were null.

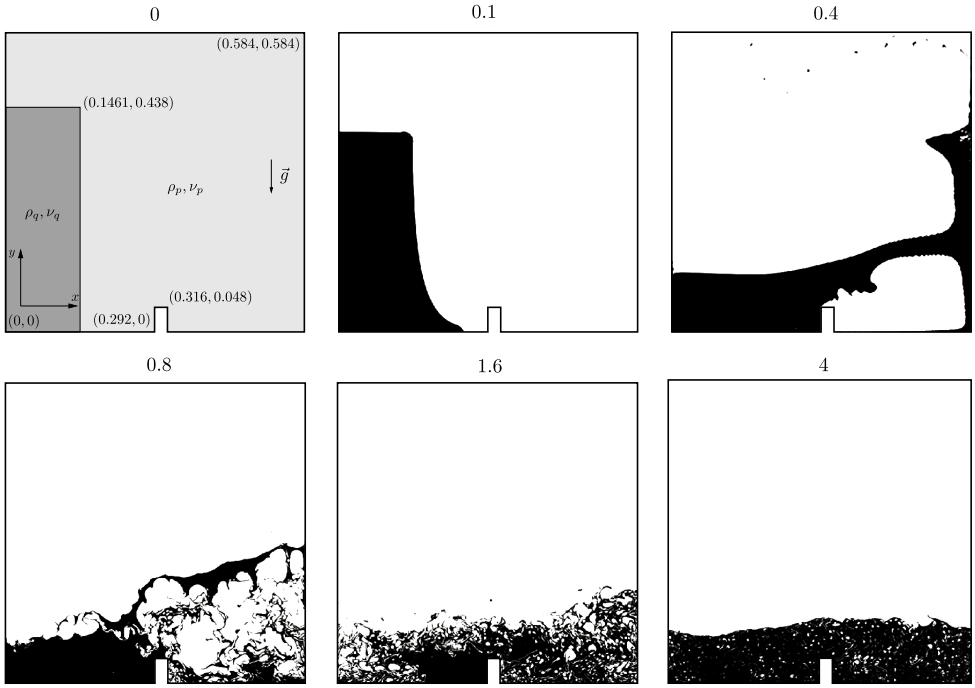


Figure 7: Evolution of the Dam Break problem

The numerical solution for the Dam Break problem is shown in Figure 7. At the beginning, the more dense fluid column collapses and pass over the obstacle until reach the right wall in a very ordered flow (up to $t = 0.7$, approximately). Once the more dense fluid reaches the right wall, it splashes forming chunks and droplets. The flow oscillates and the interface breaks in several other small interfaces trapping the less dense fluid ( $t = 1.6$). The oscillation continues as a liquid pendulum which is damped by the wall and internal friction due to the viscosity ($t \geqslant 3.4$). Finally, the system starts a quiescent stage forming a pool with the more dense fluid at the bottom layer and the less dense fluid trapped in bubbles, which are removed by buoyancy reaching a complete segregated and hydrostatic state (not shown).

It is clear that, after a first stage of mixing, the more dense fluid traps bubbles of the less dense fluid, which are lately removed by buoyancy. At the same time, droplets are formed from the splashing of the waves which fall by the gravity effects. The capacity of the VOF model to capture the physics of these particulated phases is directly related with the mesh refinement, as is shown in Figure 9. In this figure, the solution for the Dam Break problem at $t = 4$ is shown for six different meshes. The first picture ($1\times$) shows the coarsest mesh and then it is

successively refined dividing the mesh step by two in both dimensions. The expected effect is observed, as the mesh is refined the reconstruction of the trapped bubbles is improved and the buoyancy is consequently better modeled, so that, the final state as a clean pool is reached more quickly. The improvement in the surface capturing accuracy is also represented. The idea behind the mesh refinement is also to obtain a reference mesh (whenever is possible) which could be considered as a DNS solution of the problem. Since the characteristic size of the bubble population is related to the surface tension this allows to estimate a mean bubble size in order to give a relative velocity law to the ASMM. In addition this size allows to determine from which mesh size is possible to capture the bubbles individually. If the diameter of the bubbles for the Dam Break problem is estimated in $1 \times 10^{-3}$ the first mesh to start capturing them would be between the $1/32\times$ and $1/64\times$ meshes.

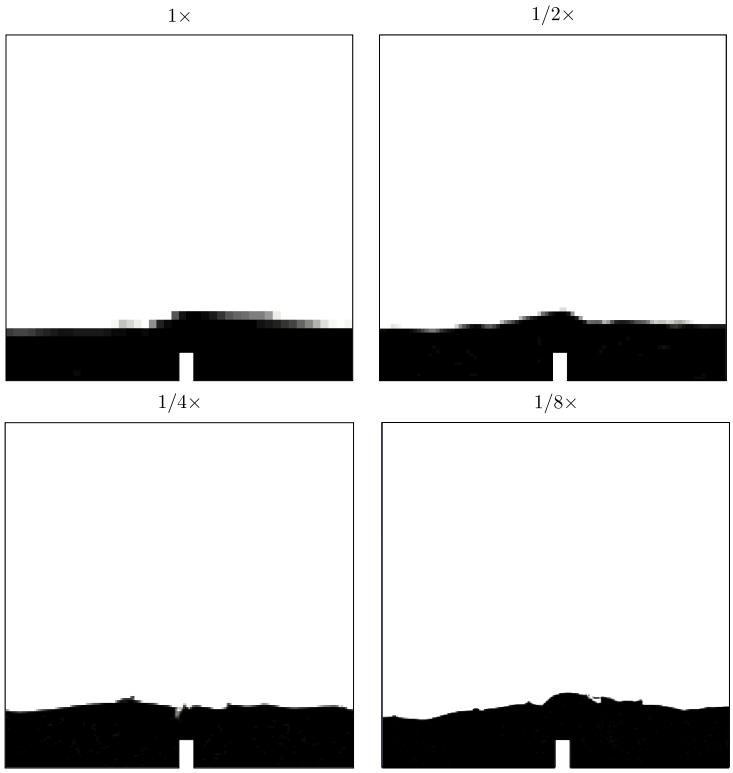


Figure 8: Extended model solution for the Dam Break problem at $t = 4$ for different meshes. The grayscale is saturated to white at $\alpha_q = 0.8$

The same analysis can be made for the extended model. It requires the selection of a relative velocity law for the particulated phase. As was stated, the Dam Break problem presents two particulated phases, droplets of the more dense phase and bubbles of the less dense phase. The selection of the dispersed phase model depends on the detection of which phase is continuous and which phase is dispersed. This is not a trivial problem and is not treated in the available methods. The dispersed phase model is then selected based on a prescribed behavior either as bubbles or droplets. Another option is to use a symmetric law for the dispersed phase model (Černe et al., 2001; Štrubelj and Tiselj, 2011), this approach has validity for $\alpha_q \sim 0.5$ since the drag laws have similar values, but is not completely correct reaching pure phases. From the figures, it is clear that is particularly necessary to give the proper physics to the trapped phase, so

that, a bubble model is selected for the relative velocity law with $a = 1$ and $\vec{v}_{rc} = (0, 0.4422, 0)$. Then, the extended model is run with $\gamma_0 = 0.1$ and $\epsilon = 5 \times 10^{-3}$ as the parameters for model coupling. The results are shown in Figure 8 where the effect of the ASMM applied to the dispersed phase is clear, the bubbles are removed giving a clear pool. The mesh refinement effect is also noted in the improvement of the free surface capturing.

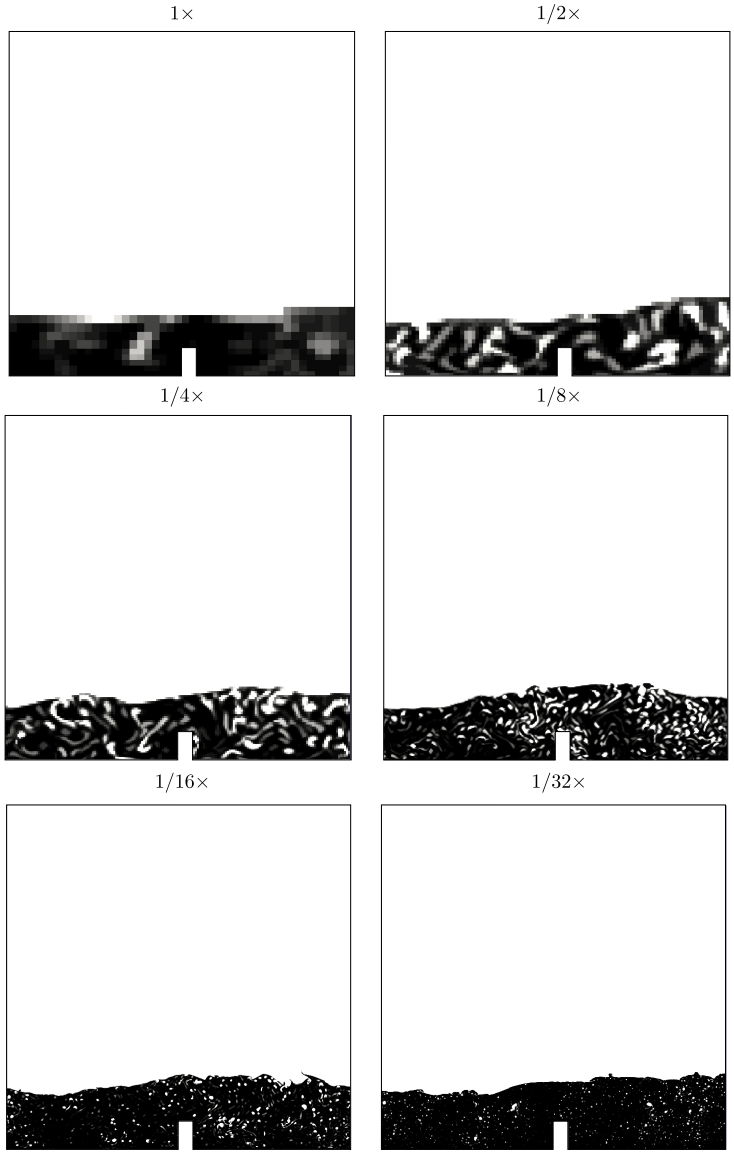


Figure 9: VOF solution for the Dam Break problem at $t = 4$ for different meshes. The grayscale is saturated to white at $\alpha_q = 0.8$

The solution for the Dam Break problem is also presented as a validation for the coupled model of Masuda and Nagaoka (Masuda and Nagaoka, 2006) (classic Dam Break, without obstacle). The authors also note the lack of capacity of VOF model to capture the bubbles and droplets and use the Two-Fluid method to give the dynamics for the particulated phase, but no quantitative validation is given with respect to this effect. A possible measure of the bubble removal is to track the inventory of the trapped phase along the time. To this end the solution for

each time-step is filtered by $p_{rgh}$ selecting only the cells with $p_{rgh} \geqslant 500$. This threshold was selected in order to capture big extensions of the more dense fluid containing either captured or non captured short scale interfaces with the less dense fluid. This subset of the whole domain is denoted $\mathcal{C}$. So that, the inventory of the less dense fluid is given by $V_p = \sum_{\mathcal{C}} (1 - \alpha_1)$. The results are shown in Figure 10 in linear and semi-logarithmic scale. The semi logarithmic scale in sub-figure b) is given in order to have a better insight of the degassing period from $t \sim 1$.

From the figure is possible to assure that the extended model has better convergence than VOF model, reaching a better degassing without increasing the refinement. It becomes clear comparing the $1/4\times$ solution for the extended model against the $1/32\times$ solution for VOF model. They show similar evolution and close level of degassing at the end of the run, giving an improvement factor of 8. Here it is important to note that the VOF mesh is 64 times larger. Following the argue the $1/8\times$ solution presented for the extended model could only be compared with a $1/256\times$ VOF solution. It implies to go from a problem of 2,008,352 cells ($1/32\times$ case) to another one with 128,534,528 cells, which is only affordable today by large HPC facilities.

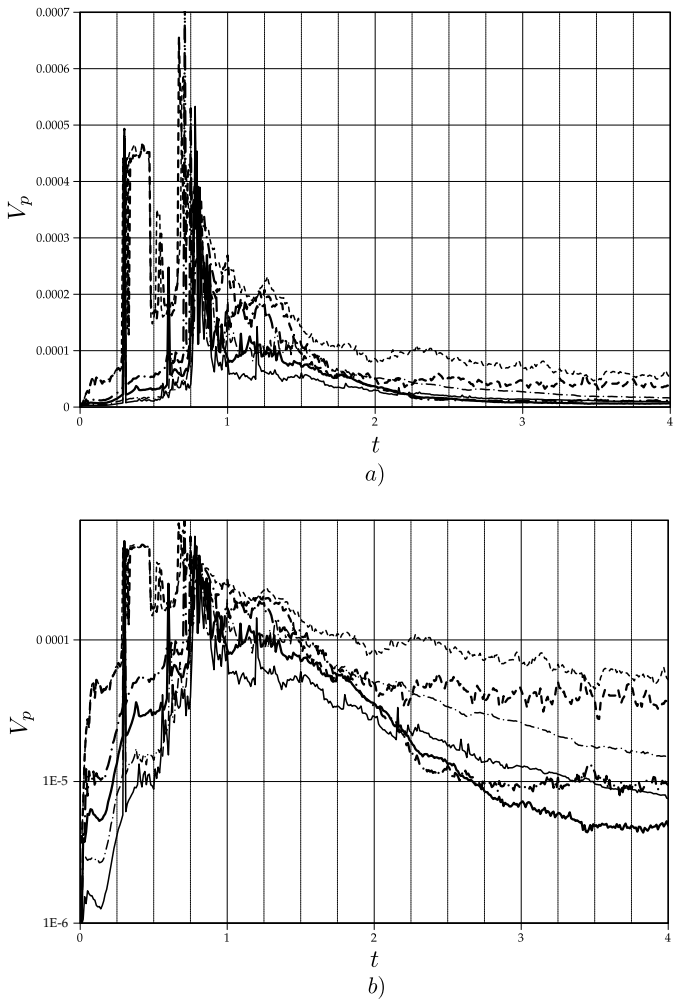


Figure 10: Evolution of the trapped phase volume, $V_p$, along the time for different meshes and models. a) linear scale, b) semi logarithmic scale. — — — — $1\times$ VOF; ——·—— $1/16\times$ VOF; ———— $1/32\times$ VOF; — — — — $1\times$ extended; ——•—— $1/4\times$ extended; ———— $1/8\times$ extended

## 5 CONCLUSIONS

In this work, an extended mixture model was presented and a high performance solver was implemented and tested in order to solve problems with different scales in the interface based on the ASMM and VOF models. To derive such model, a discussion was set about the similarities between ASMM and VOF, showing that the later can be completely derived from the first. This characteristic allowed to obtain an unified solving framework with strong coupling between the base methods and to preserve the original characteristics in the treatment of the interfaces. So that, the large scale interfaces continued to be properly captured by means of the VOF method and the short scale interfaces dynamics were treated by the ASMM. The implementation by the FVM required a careful treatment of the face fluxes in order to obtain a conservative method, this topic was explained in the theory fundamentals and was used as a key concept to devise the solver algorithm. In addition, an indicator function was presented to allow the correct coupling of both ASMM and VOF methods with a low demanding technique.

As a part of the discussion, a description of the state of the art was given in order to have a better understanding of the scope and limitations of the known coupled solvers, including the development of new theoretical and experimental solutions which allow the validation of the models.

The model was applied to two examples. The first one was an experimental bubble plume taken from the literature, giving place to a new test case. The solution of this case allowed to have a semi-quantitative validation based on the inspection of the solution and the comparison of the shape of the free-surface. This last comparison was made against fitting curves based on experimental results. The results allowed to affirm that the coupled model could correctly capture the large scale interfaces given by the pool's water surface and the fountain. The diameter of the fountain was slightly underestimated, which is attributable to the lack of turbulent diffusion in the dispersed phase. Here it is important to note that the coupled model can easily be updated including turbulent diffusion in the secondary phase mass conservation equation, which cannot be made in the VOF method since all interface scales are supposed to be solved. In addition, the trapped bubbles present in the pool, which couldn't be removed by buoyancy forces by the VOF method, were properly removed adding the correct physics by the ASMM. This effect allowed to match the observed experimental results.

The second example relied on the Dam Break problem, it was solved with the extended method and a comparison was done against the VOF model which is the typical method used to solve it. An eight times improvement was found related to mesh requirements based on a novel quantitative comparison based on the mass of the trapped phase. This example has been solved by other authors being a part of the typical test for coupled model. In this case, the proposed method showed comparable results to other methods and the utilization of improved measures allows to have more tools to evaluate the convenience of the coupled models.

As is usual, the examination of the benefits and deficiencies of this kind of methods leave some open questions to the community. An open question which deserves much attention and which has not been discussed is related to the interaction of the short scale interfaces (SSI) and the large scale interfaces (LSI). From the given examples, it is clear that the dynamics of the SSI is improved, now is necessary to know how the LSI simulation is improved due to the bet-

ter calculation of the SSI. This question is not so trivial to answer since requires very accurate validation data either theoretical or experimental.

### 5.1 Acknowledgement

The authors wish to give thanks to CONICET and Universidad Nacional del Litoral (CAI+D 2011 PI 501 201101 00435) for their financial support.

An special acknowledgment is given to OpenFOAM®, gdb, octave, Inkscape and Paraview® developers and users community for their contribution to free software.

## REFERENCES

Babik F., Gallouët T., Latché J., Suard S., and Vola D. On two fractional step finite volume and finite element schemes for reactive low mach number flows. In *The International Symposium on Finite Volumes for Complex Applications IV-Problems and Perspectives-Marrakech (2005)*. 2005.

Berberovic E., Van Hinsberg N., Jakirlic S., Roisman I., and Tropea C. Drop Impact onto a Liquid Layer of Finite Thickness: Dynamics of the Cavity Evolution. *Physical Review E*, 79, 2009.

Bohorquez P. Finite volume method for falling liquid films carrying monodisperse spheres in newtonian regime. *AIChE Journal*, 58(8):2601–2616, 2012.

Bohorquez R. de M. P. *Study and Numerical Simulation of Sediment Transport in Free-Surface Flow*. Ph.D. thesis, Málaga University, Málaga, 2008.

Brackbill J., Kothe D., and Zemach C. A continuum method for modeling surface tension. *Journal of Computational Physics*, 100(2):335–354, 1992.

Brennen C.E. *Fundamentals of multiphase flow*. Cambridge University Press, 2005.

Carrica P., Wilson R., and Stern F. An unsteady single-phase level set method for viscous free surface flows. *International Journal for Numerical Methods in Fluids*, 53(2):229–256, 2006.

Cruchaga M., Celentano D., and Tezduyar T. Collapse of a Liquid Column: Numerical Simulation and Experimental Validation. *Comput. Mech.*, 39:453–476, 2007.

Drew D. Mathematical Modeling of Two-phase Flow. *Annual Review of Fluid Mechanics*, 15(1):261–291, 1983.

Friedl M. *Bubble plumes and their interactions with the water surface*. Ph.D. thesis, Swiss Federal Institute of Technology (ETH), Zürich, 1998.

Friedl M. and Fanneløp T. Bubble plumes and their interaction with the water surface. *Applied Ocean Research*, 22(2):119–128, 2000.

Gastaldo L., Herbin R., and Latché J. An entropy preserving finite-element/finite-volume pressure correction scheme for the drift-flux model. *Arxiv preprint arXiv:0803.2469*, 2008.

Gastaldo L., Herbin R., and Latché J. A discretization of the phase mass balance in fractional step algorithms for the drift-flux model. *IMA Journal of Numerical Analysis*, 31(1):116–146, 2011.

Hirt C. and Nichols B. Volume of Fluid (VOF) Method for the Dynamics of Free Boundaries. *Journal of Computational Physics*, 39:201–225, 1981.

Ishii M. Thermo-Fluid Dynamic Theory of Two-phase Flow. *NASA STI/Recon Technical Report A*, 75, 1975.

Ishii M. and Hibiki T. *Thermo-fluid dynamics of two-phase flow*. Springer Verlag, 2010.

Issa R. Solution of Implicitly Discretised Fluid Flow Equations by Operator Splitting. *Journal of Computational Physics*, 62:40–65, 1986.

Jasak H. *Error analysis and estimation for the finite volume method with applications to fluid flows*. Ph.D. thesis, Department of Mechanical Engineering Imperial College of Science, Technology and Medicine, London, UK, 1996.

Knio O., Najm H., and Wyckoff P. A semi-implicit numerical scheme for reacting flow: II. Stiff, operator-split formulation. *Journal of Computational Physics*, 154(2):428–467, 1999.

Kolev N. *Multiphase Flow Dynamics 4: Nuclear Thermal Hydraulics*. Springer-Verlag GmbH, 2010.

Manninen M., Taivassalo V., and Kallio S. *On the mixture model for multiphase flow*. Technical Research Centre of Finland, 1996.

Márquez Damián S. *An extended mixture model for the simultaneous treatment of short and long scale interfaces*. Ph.D. thesis, FICH, Universidad Nacional del Litoral, Santa Fe, Argentina, 2013.

Martin J. and Moyce W. An Experimental Study of the Collapse of Liquid Columns on a Rigid Horizontal Plane. *Philos. Trans. R. Soc. Lond.*, 244:312–324, 1952.

Masuda R. and Nagaoka M. A Coupled Interface-capturing and Multi-fluid Model Method for Computing Liquid Jet from Nozzle Flow. In *International Congress on Liquid Atomization and Spray Systems (2006)*. 2006.

Najm H., Wyckoff P., and Knio O. A semi-implicit numerical scheme for reacting flow: I. Stiff chemistry. *Journal of Computational Physics*, 143(2):381–402, 1998.

OpenCFD. OpenCFD Technical report no. TR/HGW/02. 2005.

Peng Karrholm F. *Numerical Modelling of Diesel Spray Injection, Turbulence Interaction and Combustion*. Ph.D. thesis, Chalmers University of Technology, Goteborg, 2008.

Prosperetti A. and Tryggvason G. *Computational methods for multiphase flow*. Cambridge University Press, 2007.

Puckett E., Almgren A., Bell J., Marcus D., and Rider W. A high-order projection method for tracking fluid interfaces in variable density incompressible flows. *Journal of Computational Physics*, 130(2):269–282, 1997.

Rudman M. Volume-tracking Methods for Interfacial Flow Calculations. *International Journal for Numerical Methods in Fluids*, 24(7):671–691, 1997.

Rusche H. *Computational Fluid Dynamics of Dispersed Two-Phase Flows at High Phase Fractions*. Ph.D. thesis, Imperial College of Science, Technology and Medicine, London, 2002.

Scardovelli R. and Zaleski S. Direct Numerical Simulation of Free-Surface and Interfacial Flow. *Annual Review of Fluid Mechanics*, 31(1):567–603, 1999.

Schiller L. and Naumann Z. A drag coefficient correlation. *Z. Ver. Deutsch. Ing.*, 77:318, 1935.

Spalart P., Jou W., Strelets M., and Allmaras S. Comments on the feasibility of LES for wings, and on a hybrid RANS/LES approach. *In Advances in DNS/LES*, pages 137–147, 1997.

Spalart P.R. Detached-eddy simulation. *Annual Review of Fluid Mechanics*, 41:181–202, 2009.

Tryggvason G., Esmaeeli A., Lu J., and Biswas S. Direct Numerical Simulations of Gas/liquid Multiphase Flows. *Fluid Dynamics Research*, 38(9):660–681, 2006.

Černe G., Petelin S., and Tiselj I. Coupling of the Interface Tracking and the Two-fluid Models for the Simulation of Incompressible Two-phase Flow. *Journal of Computational Physics*, 171:776–804, 2001.

Štrubelj L. and Tiselj I. Two-fluid Model with Interface Sharpening. *International Journal for Numerical Methods in Engineering*, 85(5):575–590, 2011.

Weller H. A new approach to VOF-based interface capturing methods for incompressible and

compressible flow. 2008.

Yan K. and Che D. A Coupled Model for Simulation of the Gas-liquid Two-phase Flow with Complex Flow Patterns. *International Journal of Multiphase Flow*, 36(4):333–348, 2010.

Zalesak S. Fully Multidimensional Flux-Corrected Transport Algorithms for Fluids. *Journal of Computational Physics*, 31:335–362, 1979.

Zanotti A.L. *Modelado del Flujo Multifase en la Produccion de Acero por Colada Continua*. Ph.D. thesis, Facultad de Ingeniería y Ciencas Hídricas, UNL. Santa Fe, Argentina, 2007.